Published in "Advanced Functional Materials doi: 10.1002/adfm.201904007, 2019"
which should be cited to refer to this work.

# Multifunctional Nano-Biointerfaces: Cytocompatible Antimicrobial Nanocarriers from Stabilizer-Free Cubosomes

*Mahsa Zabara, Berna Senturk, Mark Gontsarik, Qun Ren, Markus Rottmar, Katharina Maniura-Weber, Raffaele Mezzenga, Sreenath Bolisetty, and Stefan Salentinig**

**The rational design of alternative antimicrobial materials with reduced toxicity toward mammalian cells is highly desired due to the growing occurrence of bacteria resistant to conventional antibiotics. A promising approach is the design of lipid-based antimicrobial nanocarriers. However, most of the commonly used polymer-stabilized nanocarriers are cytotoxic. Herein, the design of a novel, stabilizer-free nanocarrier for the human cathelicidin derived antimicrobial peptide LL-37 that is cytocompatible and promotes cell proliferation for improved wound healing is reported. The nanocarrier is formed through the spontaneous integration of LL-37 into novel, stabilizer-free glycerol monooleate (GMO)-based cubosomes. Transformations in the internal structure of the cubosomes from *Pn3m* to *Im3m*-type and eventually their transition into small vesicles and spherical micelles are demonstrated upon the encapsulation of LL-37 into their internal bicontinuous cubic structure using small angle X-ray scattering, cryogenic transmission electron microscopy, and light scattering techniques. Additional in vitro biological assays show the antimicrobial activity of the stabilizer-free nano-objects on a variety of bacteria strains, their cytocompatibility, and cell-proliferation enhancing effect. The results outline a promising strategy for the comprehensive design of antimicrobial, cytocompatible lipid nanocarriers for the protection and delivery of bioactive molecules with potential for application as advanced wound healing materials.**



Dr. M. Zabara, Dr. B. Senturk, M. Gontsarik, Dr. Q. Ren, Dr. M. Rottmar, Prof. K. Maniura-Weber, Prof. S. Salentinig
Laboratory for Biointerfaces
Department of Materials Meet Life
Empa, Swiss Federal Laboratories for Materials Science and Technology
Lerchenfeldstrasse 5, 9014 St. Gallen, Switzerland
E-mail: stefan.salentinig@unifr.ch

Prof. R. Mezzenga, Dr. S. Bolisetty
Laboratory for Food and Soft Materials
Institute of Food, Nutrition and Health
ETH Zurich
Schmelzbergstrasse 9, 8092 Zürich, Switzerland

Prof. S. Salentinig
Department of Chemistry
University of Fribourg
Chemin du Musée 9, 1700 Fribourg, Switzerland

## 1. Introduction

Antibiotic resistant bacteria are a growing concern in the medical field, posing a high demand in finding alternative strategies to fight bacteria. Antimicrobial peptides (AMPs) are a promising alternative to classical antibiotics.[1] AMPs exert multiple antibacterial mechanisms including destabilization of the bacterial membrane, which makes it less likely that bacteria can develop resistance toward them.[2] However, acting as an antimicrobial agent is not the only important task of AMPs. These peptides appear to play an important role in many aspects of innate immunity and the inflammatory response.[3] On the molecular level, AMPs represent a group of short and mostly positively charged peptides found in the widespread form of lives from micro-organism to human. The only AMP from the cathelicidin family found in the human body is LL-37.[4] Possessing antimicrobial effects while enhancing cell migration and proliferation makes AMPs such as LL-37 a desirable therapeutic agent for medical applications such as wound-healing.[5] However, the inherent complex properties of AMPs, including their low solubility in water, and their low stability in the biological environment result in low bioavailability and have hindered their broader therapeutic application.[6]

One of the most promising approaches to address these issues is to encapsulate AMPs into suitable nanocarriers to protect and transport them in the aqueous biological environment.[7] Recently, dispersions of inverse liquid crystalline nanocarriers based on amphiphilic lipids such as glycerol mono-oleate (GMO) were designed for this purpose.[8] The broadly active LL-37 was demonstrated to spontaneously integrate into the internal nanostructure of triblock-copolymer stabilized, GMO[8d] and oleic acid (OA) based nanoparticles[8e] when added to the aqueous phase of the dispersions. The polymer-stabilized GMO/LL-37 self-assemblies were discovered to exhibit significant antibacterial activity, eliminating a Gram-negative *Escherichia coli* (*E. coli*) bacteria strain faster and more efficiently than free LL-37.[8d]

The triblock copolymer F127 is commonly used as a stabilizer for such nanoparticles in the aqueous environment.[9] However, potential concentration-dependent cytotoxicity, hemolytic properties, and poor biodegradability of F127 may limit the clinical application of the F127 stabilized nanoparticles.[9e,10] It was reported that F127 activates the human complement system in both micellar and surface immobilized forms.[11] The corresponding cytotoxic properties of F127 stabilized lipid-based drug delivery vehicles such as cubosomes and hexosomes have been addressed in detail in the literature.[9e,10a,b,d,12]

The major goal of this study is to design novel, stabilizer-free antimicrobial nanocarriers that are cytocompatible and promote cell proliferation for improved wound healing. The novel stabilizer-free cubosomes were designed by dispersing the GMO bulk phase in water using ultrasonication with an optimized dispersion protocol. The resulting stabilizer-free cubosomes were found colloidally stable for at least several weeks. The following addition of LL-37 to the aqueous phase of the dispersion led to the spontaneous integration of LL-37 into the interior of the cubosomes and their transformation into cytocompatible antimicrobial nanocarriers that further promoted cell proliferation. Small angle X-ray scattering (SAXS), (depolarized) dynamic light scattering ((D)DLS), and cryogenic transmission electron microscopy (cryo-TEM) were used to investigate nanostructure, morphology, and stability of the self-assembled nanocarriers. Antibacterial assays against clinically relevant bacterial strains of both Gram-positive and Gram-negative types including *Pseudomonas aeruginosa (P. aeruginosa), E. coli, Staphylococcus aureus (S. aureus), Staphylococcus epidermis (S. epidermis), and Bacillus subtilis (B. subtilis)* were performed to evaluate the antimicrobial activity of the nano-objects, whereas potential cytotoxicity and effects on cell proliferation were studied with primary human dermal fibroblasts (HDF) and a human monocytic leukemia cell line (THP-1).

## 2. Results and Discussion

### 2.1. Characterization of Binary Self-Stabilized GMO/LL-37 Nanostructures

GMO-based cubosomes were prepared in the absence of any hydrophilic stabilizer by dispersing GMO in water using ultrasonication. The SAXS scattering curves of these stabilizer-free cubosomes before and after integration of the LL-37 are demonstrated in **Figure 1**. Before the addition of LL-37, the first four Bragg reflections of an inverse diamond-type bicontinuous cubic phase (*Pn3m* type) with a lattice parameter of ≈10 nm were observed. This dispersed nanostructure agrees with the nondispersed GMO bulk phase in excess water.[13] In contrast, GMO-based dispersion stabilized by F127 showed a primitive-type cubic structure (*Im3m* type) due to the interaction of F127 with the internal lipid structure.[8d,f,g,9c] Representative cryo-TEM images for these stabilizer-free nanocarriers are presented in **Figure 2**a. The images show the presence of cubosomes in the absence of any F127. A lamellar layer appears to envelop the internal bicontinuous cubic phase of the stabilizer-free cubosomes and help stabilizing the nanoparticles. This outer layer may be formed by local gradients in a composition close

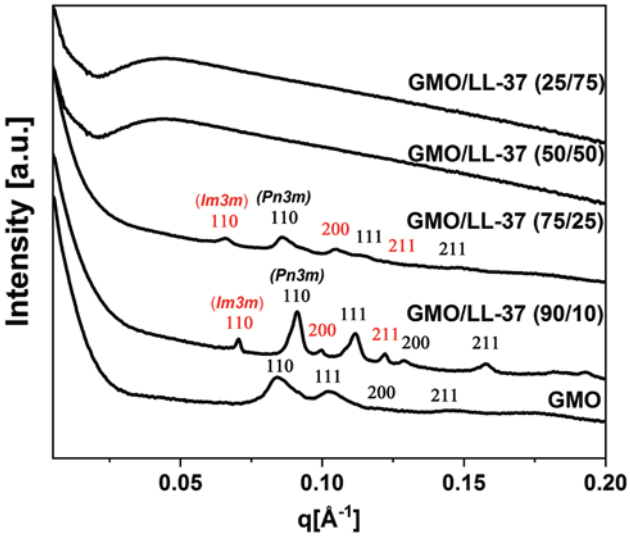


**Figure 1.** SAXS patterns of the GMO/LL-37 self-assemblies in the absence of secondary stabilizer in water. The identifiable Bragg peaks are indexed with the corresponding Miller indices. The $I(q)$ data for self-stabilized GMO cubosomes, before the addition of LL-37, show the scattering pattern of the *Pn3m* phase. At GMO/LL-37 ratios of 90/10 and 75/25, scattering patterns of coexistence of *Pn3m* and *Im3m* phases were observed. The Bragg reflections of the highly ordered structures diminish at GMO/LL-37 ratios of 50/50 and 25/75, and the scattering patterns indicate the formation of vesicles.

to the particle surface, potentially by the presence of small amounts of free fatty acids that can be released during the preparation process. In this context, free fatty acids such as oleic acid were previously used as a stabilizer for internally nanostructured particles.[14] To exclude the effect of impurities in the technical-grade GMO as stabilizers for the nanoparticles, the cubosomes were prepared with both, technical-grade GMO (≥90% purity) and highly pure GMO (>99% purity). No significant differences in the nanostructure and nanoparticle stability were observed between the batches of different purity.

DLS measurements on stabilizer-free cubosomes performed directly after preparation and 21 d after preparation confirm the colloidal stability of the particles within this time frame, with $R_H \approx 215$ nm (PDI 0.21) and $R_H \approx 270$ nm (PDI 0.20), respectively. The corresponding correlation functions, presented in Figure S2 (Supporting Information), show rather monomodal particle size distributions with one dominating decay. The scattered intensity at 90° slightly decreased from 244 to 229 kps over 21 d, indicating that the concentration of the particles slightly decreased. This can result from particle aggregation and separation and is not reflected in the PDI as only the first decay of the correlation functions in Figure S2 (Supporting Information) was fitted with the cumulant method.

The addition of LL-37 to the stabilizer free GMO-cubosomes resulted in significant alterations in the internal particle structure (Figure 1). At GMO/LL-37, 90/10 w/w ratio the Bragg reflections of the *Pn3m* structures shift to higher $q$-values, indicating a slightly smaller lattice parameter of ≈9.7 nm. Additional Bragg peaks appear in these samples and are most likely attributed to a coexisting inverse bicontinuous cubic *Im3m* phase with a lattice parameter of ≈12 nm (Figure 1). Further,

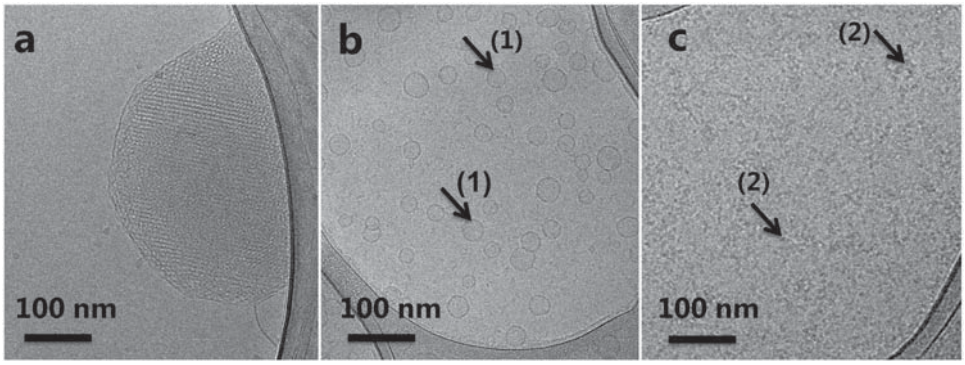


**Figure 2.** Cryo-TEM images of the nanocarriers at GMO/LL-37 ratios of a) 100/0 w/w ratios (stabilizer-free cubosomes in water). The lamellar layer at the particle surface likely helps the cubosomes' stabilization; b,c) 50/50 w/w ratios. The highly ordered structures disappeared, and small vesicles (1) and micelles (2) can be observed.



increase in the LL-37 content to a GMO/LL-37 weight ratio of 75/25 induced a shift of the Bragg reflections to lower *q*-values and decrease in their intensity. At even higher LL-37 content at a GMO/LL-37 weight ratio of 50/50 and 25/75, scattering patterns indicative of vesicles can be observed. The pair-distance distribution function *p(r)* calculated from the SAXS data using the indirect Fourier transformation method is characteristic for locally flat structures (vesicles) as it is known from simulations (see Figure S1, Supporting Information).[15] This is further supported by the $q^{-2}$ upturn of the $I(q)$ at low *q*-values that is also characteristic for these structures at GMO/LL-37 of 50/50 (see Figure S1, Supporting Information).

The cryo-TEM image for the sample at GMO/LL-37 weight ratio of 50/50 further confirms the presence of vesicles of various sizes and shapes potentially coexisting with small micelles (see Figure 2b,c). However, the presence of bilayer sheets or bicelles, as well as elongated micelles, cannot be excluded as they are difficult to distinguish from the objects observed in these images. To investigate the presence of optically anisotropic particles such as bicelles or elongated micelles, DDLS measurements were performed on both, the GMO/LL-37 and GMO/LL-37/F127 system (**Figure 3**). Interestingly, the DDLS results revealed negligible anisotropic scattering for the GMO/LL-37 sample, whereas considerable depolarized scattering was observed for the GMO/LL-37/F127 system. This suggests that F127 stabilizes the formation of anisotropic structures such as bicelles or elongated micelles in this system demonstrating that F127 not only acts as a stabilizer but also actively participates in the self-assembly process.

The structural transformation from highly geometrically ordered structures to vesicles and micelles upon the encapsulation of LL-37 was discovered in the stabilizer-free GMO/LL-37 nanoparticles as well as in the F127 stabilized system.[8d] However, the stabilizer-free cubosomes presented in this study maintain their highly ordered nanostructure up to a GMO/LL-37 weight ratio of 75/25. On the contrary, the F127 stabilized systems transform to low-order structures already at a GMO/LL-37 ratio of 90/10, which can be attributed to the F127-induced increase in the hydrophilic headgroup area at the internal oil–water interface that results in swelling of the cubic structure.[16]

### 2.2. Antibacterial Studies

The antibacterial properties of the formulation (GMO/LL-37) were investigated in vitro using minimum inhibition concentration (MIC) evaluations (Table S1, Supporting Information), and time-kill assays (**Figure 4**) against the five different bacteria strains *P. aeruginosa, E. coli, S. aureus, S. epidermis, and B. subtilis*. The stabilizer-free nanocarriers appeared to be highly efficient in inhibiting the growth of *E. coli and P. aeruginosa* at even lower concentrations compared to the F127 containing formulation and the free LL-37: For *E. coli* the MIC was ≤40 μg $mL^{-1}$ for the GMO/LL-37 nanocarriers and ≤80 μg $mL^{-1}$ for GMO/LL-37/F127, and for *P. aeruginosa* the MIC was ≤32 μg $mL^{-1}$ for the GMO/LL-37 and ≤64 μg $mL^{-1}$ for GMO/LL-37/F127 system (Table S1, Supporting Information). Interestingly, both, the F127 containing and F127-free formulations, did not exhibit significant antibacterial properties against any of the studied Gram-positive bacteria strains (*S. aureus, S. epidermis*, and *B. subtilis*), even up to 250 μg $mL^{-1}$ of LL-37. This significant difference in antibacterial performance against the Gram-negative and Gram-positive bacteria is likely due to the different cell-wall structures of the bacteria types, as Gram-positive bacteria possess a much thicker peptidoglycan layer within the cell membrane, compared to Gram-negative bacteria.[17] These peptidoglycan layers are differently structured with a higher crosslinking density in Gram-positive bacteria and potentially limit the access of LL-37 encapsulated in the nanoparticles to the lipid membrane, an action that is a prerequisite for the antibacterial activity of LL-37.[18] The observed selectivity of the antibacterial behavior against Gram-negative bacteria strains could be interesting for treating digestive tract infections. Gram-positive bacteria such as probiotics are the predominant micro-organisms found in the small intestine, and they aid a wide range of intestinal functions.[19] Preserving the Gram-positive bacteria while eliminating infections caused by Gram-negative bacteria could improve therapies by reducing the side effects from eliminating probiotic bacteria.

To further investigate the antimicrobial activity against the Gram-negative bacteria, time-kill assays were performed with the nanocarriers against *E. coli* and *P. aeruginosa* at LL-37 concentrations in a range of 8–64 μg $mL^{-1}$ during a time interval of 20 h (see Figure 4a,c). In agreement with the results obtained

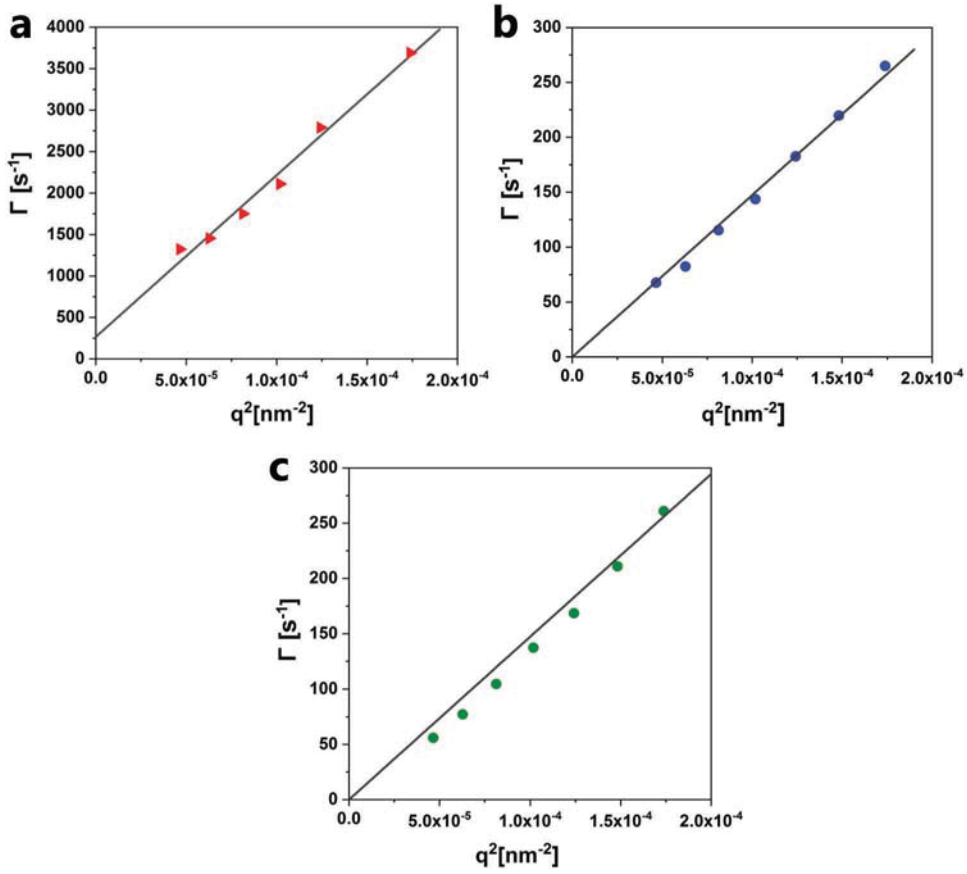


**Figure 3.** DLS and DDLS measurement conducted for GMO/LL-37 at 50/50 w/w ratio in the presence and absence of F127. a) The sample containing F127 had significant scattering in depolarized (vertical horizontal, VH) mode with count rates up to 1000 kHz, which indicates that the structures are anisotropic in shape (i.e., bicelles). The angular-dependent measurement indicates a rotational diffusion coefficient of 44 rotations $s^{-1}$. b) Angular-dependent decay rate measured in polarized (vertical, VV) mode for the GMO/LL-37/F127 system resulted in a translational diffusion coefficient of $1.47 \times 10^6$ $nm^2$ $s^{-1}$. c) In the absence of F127, the angular dependence of the decay rate in polarized (VV) mode for the GMO/LL-37 system also resulted in a translational diffusion coefficient of $1.47 \times 10^6$ $nm^2$ $s^{-1}$. The scattering intensity in depolarized (VH) mode was not significant, which indicates the isotropic nature of these particles. All experiments were performed at room temperature.

from the MIC studies, the "F127-free" GMO/LL-37 assemblies showed higher antibacterial activity compared to the GMO/LL-37/F127 system. In the absence of F127, the GMO/LL-37 nano-objects at the final LL-37 concentration of 64 μg $mL^{-1}$ led to a 6-log reduction after 60 min for *E. coli* and after 180 min for *P. aeruginosa* (Figure 4b,d, respectively). On the contrary, the F127 containing formulations showed only a 1 log reduction toward *E. coli* and less than 3 log reduction toward *P. aeruginosa* after 180 min. After 1200 min there were even more viable *E. coli* cells than the original cell numbers, indicating insufficient antibacterial activity of F127 containing formulations and regrowth of bacteria.

The distinct differences in antimicrobial activity between the formulations with and without F127 may be caused by the different nanocarrier surface structure, charge and shape. The higher ζ-potential of +18 mV in phosphate buffer saline (PBS) for the stabilizer-free formulations, compared to a ζ-potential of +12 mV in PBS for the formulations with F127 may induce stronger attraction forces between the complexes and the negatively charged bacterial membrane. The importance of electrostatic interaction in the accumulation of cationic components at the negatively charged bacterial membrane has been reported previously.[2a,20] Further, in the GMO/LL-37/F127 system, the hydrophilic PEO blocks of the F127 may form a polymeric brush-like coating around the particle that can sterically hinder the contact of LL-37 with the lipid bilayer or even entrap the particles in the lipopolysaccharide matrix in the outer bacterial membrane.[21] Also, the nanoparticle geometry has been reported to affect their interaction with a lipid bilayer (cell-wall).[22] The internalization of anisotropic structures such as discs or elongated micelles into bilayers can be further delayed by an unfavorable docking orientation since a time-consuming rotation is required to achieve the alignment.[22b,23] As the F127 containing systems were found to be anisotropic in shape, this likely contributed to reducing their antimicrobial activity compared to the isotropic nano-objects in the absence of F127.

### 2.3. Cell Viability and Proliferation Study

The toxicity and cell-proliferation activity of the nanocarriers was studied on two different cell lines: HDF cells and THP-1.

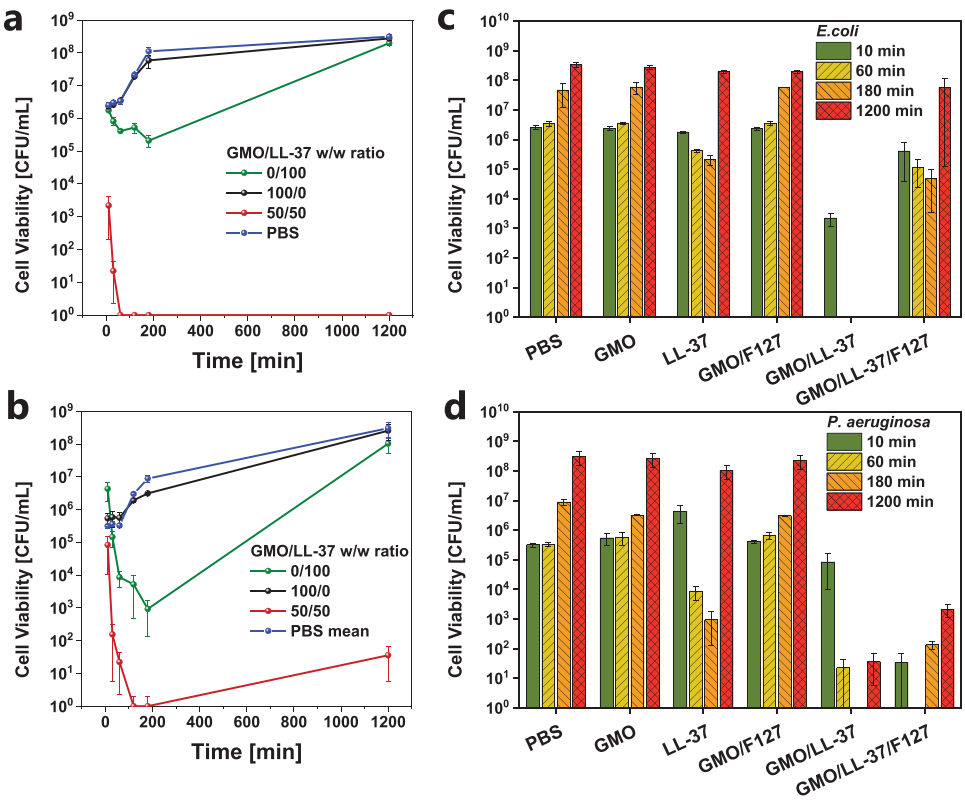


**Figure 4.** Antibacterial activity of GMO/LL-37 self-assemblies against a) *E. coli* and b) *P. aeruginosa* over 1200 min of exposure. The bacterial culture was treated with 64 μg mL free LL-37 in solution (positive control (0/100) or as part of selected self-assembled nanostructures as indicated). c,d) Comparison of the antibacterial activity of the GMO/LL-37 and the GMO/LL-37/F127 systems against c) *E. coli* and d) *P. aeruginosa*. PBS, GMO, GMO/F127, and LL-37 were used as controls. Antimicrobial assays indicate that the GMO/LL-37 self-assemblies induce up to 100% bacterial death for both strains after 180 min of exposure without significant regrowth of bacteria up to 1200 min (panels c and d). On the contrary, free LL-37 at the same concentration as in the formulations of 64 μg $mL^{-1}$ only resulted in 60% death for *E. coli* and 30% for *P. aeruginosa* after 180 min. The number of viable bacteria increased again after 1200 min N = 3.

HDF cells are crucial components in the process of wound healing. They maintain the physical integrity of the connective tissue, participate in wound closure as well as produce and remodel extracellular matrix.[24] Investigation of the cytotoxic effect of a nanocarrier system on fibroblasts is therefore crucial in this context. Macrophages derived from human monocytes are also essential and dominant cells during wound healing.[25] they have a close relationship with fibroblasts by increasing the production of matrix metalloproteinase-1 as well as influencing fibroblast to myofibroblast differentiation for faster wound closure and remodelling.[24]

The HDF cell viability with both systems was assessed in vitro with an Alamar Blue assay after 24 and 72 h, and additionally with a Live/Dead assay after 72 h (**Figure 5** and Figure S3, Supporting Information). The Live/Dead assay in Figure 5a indicates that the stabilizer-free GMO/LL-37 vesicles and micelles at 50/50 weight ratio are nontoxic to HDF cells. On the contrary, the GMO/LL-37/F127 self-assemblies appear cytotoxic with dead HDF cells in red. The unloaded GMO cubosomes follow this trend with fewer dead cells in the stabilizer-free cubosomes (GMO) compared to the F127 stabilized cubosomes (GMO/F127) (Figure S3, Supporting Information). The complementary Alamar Blue assay agrees well with the results from the Live/Dead assay: The stabilizer-free GMO/LL-37 self-assemblies appear nontoxic with cell viability of 83.01 ± 11.64% after 24 h and only a slight decrease to values above 80% after 72 h (Figure 5b). The F127 stabilized nanocarriers on the other hand are cytotoxic, with HDF viability showing significantly lower values of 73.62 ± 8.20% after 24 h and 19.00 ± 4.40% after 72 h. Contrary to the surface-bound F127 in the nanocarriers, free F127 at the same concentration (0.1% w/v), which is below the reported critical micellar concentration (CMC) of F127 (0.725 w/v at 25 °C), does not appear to be cytotoxic (Figure 5b, control).[26]

LL-37 has further been reported to have a positive effect on wound healing by stimulating proliferation.[3b,27] Therefore, the impact of the nanocarrier structures on the proliferation of HDF cells was studied 24 h after treatment. The HDF cells were stimulated with the GMO/LL-37 and GMO/LL-37/F127 nanocarriers, as well as the individual components as controls.

The free LL-37 and even more the GMO/LL-37 self-assemblies significantly increased the proliferation of HDF cells compared to PBS control (Figure 5c). In contrast, the treatment with LL-37/F127 and GMO/LL-37/F127 did not increase cell proliferation.

To further elucidate the effects of the self-assemblies on HDF cell proliferation, cell uptake studies were performed with

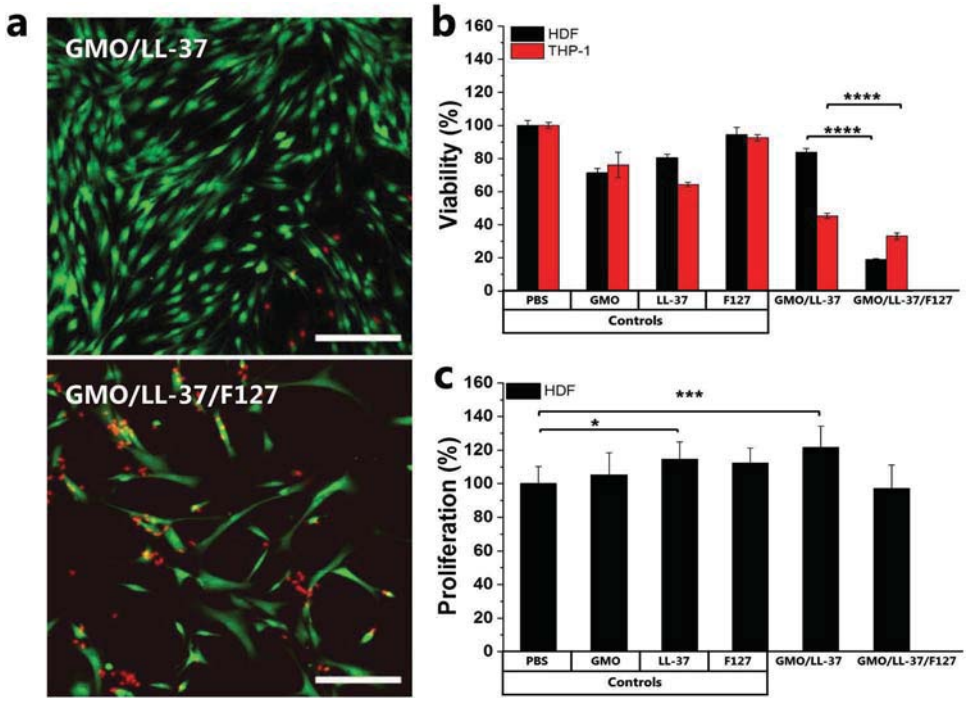


**Figure 5.** Cytotoxicity (HDF, THP-1) and proliferation (HDF) of cells treated with the GMO/LL-37 self-assemblies in the presence and absence of F127 with the relevant controls. a) The Live/Dead assay shows live cells in green (calcein-AM staining) and dead cells in red (ethidium homodimer staining). b) The GMO/LL-37 self-assemblies at 50/50 weight ratio appear nontoxic for HDF cells, contrary to the GMO/LL-37/F127 system after 72 h. c) The Alamar Blue assay also confirms that the stabilizer-free GMO/LL-37 self-assemblies are nontoxic for HDFs after 72 h, see bars as a guide for the eye. The cell proliferation of HDF indicates that the proliferation is promoted by LL-37 and GMO/LL-37 after 24 h. Scale bar; 200 μm. * $p < 0.05$, ** $p < 0.01$, *** $p < 0.001$, and **** $p < 0.0001$.

confocal microscopy using fluorescent (FAM) labeled LL-37. The FAM labelled LL-37 nanocarriers in presence and absence of F127 were administered to HDF cells and their interactions visualized after 24 h. The confocal microscopy images in Figure S5 (Supporting Information) indicate a higher uptake of the FAM labeled LL-37 when formulated in GMO/LL-37 self-assemblies compared to free LL-37. This result shows that the elevated cell proliferation observed for the GMO/LL-37 system is caused by the enhanced uptake of the LL-37 into the HDF cells. Intriguingly, the uptake of LL-37/F127 and GMO/LL-37/F127 was comparable to that of the GMO/LL-37 in this experiment. This indicates that the decrease in cell proliferation in the presence of F127 might be caused by their cytotoxicity, which outperforms the stimulating effect of LL-37 in these systems. However, detailed biochemical evaluation studies are necessary to unravel the mechanisms behind the improved cell proliferation of GMO/LL-37 nanocarriers.

## 3. Conclusion

This study demonstrates the design and characterization of cytocompatible LL-37 nanocarriers with antimicrobial and cell-proliferation enhancing properties. The nanocarriers were prepared via the spontaneous integration of the antimicrobial peptide LL-37 into the internal nanostructure of the novel, stabilizer-free GMO-based cubosomes. To the best of our knowledge, this is the first demonstration of stabilizer-free cubosomes that are further applied as LL-37 nanocarriers. Upon increasing the LL-37 content in the stabilizer-free GMO/LL-37 nanocarriers, transformations from *Pn3m* to *Im3m* type cubosomes and further to small vesicles and micelles were observed. The GMO/LL-37 at 50/50 weight ratio in the form of vesicles and micelles showed substantial antibacterial activity. Interestingly, this activity was mainly against the Gram-negative bacteria strains-, and not against the Gram-positive strains in this study. Cell viability studies on HDF and THP-1 cells demonstrated that the stabilizer-free cubosomes and nanocarriers are nontoxic, contrary to the commonly used F127 stabilized systems that were found cytotoxic. In addition, cell proliferation assays on HDF cells showed that the GMO/LL-37 nanocarriers increase cell proliferation potentially by enhancing the cellular uptake of the LL-37. Hence, the GMO/LL-37 nanocarriers are promising multifunctional biointerfaces, combining antibacterial properties with the promotion of cell proliferation, for instance, to boost wound healing. Further, the stabilizer-free cubosomes demonstrated in this study hold great promise for the design of advanced cytocompatible nanovehicles for food and drug delivery.

## 4. Experimental Section

*Sample Preparation*: Stabilizer-free cubosomes were prepared by dispersing GMO (with a purity ≥90% from Riken Vitamin Co., Ltd, Japan) and highly pure with >99% from Sigma-Aldrich, Buchs, Switzerland) in ultrapure water (resistivity > 18 MΩ cm). The technical

grade GMO typically contains 99% monoglycerides and 1% diglycerides. The fatty acid composition in the monoglycerides is dominated by oleic acid (>90%) with residual amounts of fatty acids such as linoleic acid, stearic acid, palmitic acid. The dispersions were prepared at a final concentration of 1% w/v by ultrasonication with a tip sonicator (Sonics Vibra Cell VCX 130 W, 20 kHz, Sonics & Materials Inc., Newton, CT, USA). Two cycles of ultrasonication for 5 min in pulse mode (3 s pulse, 2 s break) at 25% of maximum amplitude were applied to obtain a stable GMO dispersion.

F127 stabilized cubosomes were prepared by dispersing the GMO (≥90% purity, Riken Vitamin co., Ltd company, Japan) in $40 \times 10^{-3}$ M PBS at pH 6.5 with 0.1% w/v Pluronic F127 (BASF, Ludwigshafen, Germany) at a final concentration of 1% w/v by ultrasonication. Three cycles of ultrasonication consisted of 1 min in pulse mode (1 s pulse, 1 s break) at 20% of maximum amplitude, 2 min in pulse mode (3 s pulse, 2 s break) at 25% of maximum amplitude and 2 min in pulse mode (3 s pulse, 2 s break) at 27% of maximum amplitude were applied.

The prepared dispersions were equilibrated at 25 °C for at least 12 h before further experiments. The AMP LL-37 (99.77% purity, CASLO ApS, Lyngby, Denmark) was added to the aqueous phase of the dispersion at various weight ratios of GMO/LL-37 between 100:1 and 25:75, and the samples were further equilibrated for a minimum of 2 h before further studies.

*Methods: cryo-TEM*: Characterization of the nano-self-assemblies in their hydrated state was carried out on a Tecnai F20 cryo-TEM (FEI, USA). 300-mesh lacey carbon-coated copper grids (Quantifoil, Germany) were glow discharged (Emitech K100X, GB) for 30 s. A volume of 3 µL of sample solution was applied onto the grids in a Vitrobot Mark II (FEI, USA) and the excess of the dispersion was removed by controlled blotting. A mixture of liquid ethane/propane was used for sample vitrification. The grids were then transferred on a Gatan cryo-holder into the microscope and kept at −180 °C during observation. Micrographs were recorded under low dose conditions (<500 $e^{-}$ $nm^{-2}$) using an FEI Falcon II camera, operating the microscope at 200 kV acceleration voltage in bright field mode.

*(D)DLS and ζ-Potential*: The hydrodynamic radius ($R_H$) and polydispersity index (PDI) of different GMO/LL-37 nano-self-assemblies were determined using Malvern Zetasizer Nano ZS90 (Malvern Instruments, USA) with a He-Ne Laser beam at a wavelength of 633 nm and laser power of 4 mW with a detection angle of 90° in optically homogenous polystyrene cells. The $R_H$ was determined via cumulant analysis of the correlation function, and the PDI was estimated from the second cumulant, similar to our previous studies.[28] All measurements were performed at 25 °C. Each value is the mean of three different runs with 15 measurements each. All samples were diluted with water in the ratio of 1:10 before measurements. ζ-potential measurements were performed on the 1:10 diluted samples and their electrophoretic mobility $\mu_e$ was measured by applying 5 mV electric potential across the sample. DDLS measurements were performed on an LS Instruments (Fribourg, Switzerland) dynamic light scattering system equipped with a He–Ne Laser emitting a polarized light beam with 633 nm wavelengths. The primary beam and the scattered beam had to pass through crossed Glan-Thomson polarizers with an extinction coefficient better than $10^{-5}$. The primary beam consisted of only vertically polarized laser light. The polarizer for the scattered beam was carefully adjusted to a crossed position with minimum intensity. Correlation functions were collected at different scattering angles between 30° and 140°. At each angle, measurements over 300 s were performed, and the average of data sets was taken to obtain at least three repetitions per scattering angle. In DDLS the scattering is due to optically anisotropic particles. Here, decay rate of the field correlation function is given by

$$\Gamma = q^2 D_T + 6 D_R \quad (1)$$

$\Gamma$ being the decay rate of the depolarized field correlation function $\left(g_1^{VH}(t)\right)$. $\Gamma$ was determined from the correlation function with the CONTIN method, as described in a previous study.[29] The resulting values for $\Gamma$ were plotted versus the square of the scattering vector magnitude ($q^2$) and the translational and rotational diffusion coefficient ($D_T$ and $D_R$) for the anisotropic particles are evaluated by linear regression.[30]

*Synchrotron SAXS*: SAXS experiments were performed at the I22 SAXS beamline (Diamond Light Source synchrotron facility, Oxfordshire, UK) at operating photon energy of 12.4 keV and X-ray wavelength of 0.9999 Å. The sample to detector distance of 3563 mm provided with a $q$ range ($q = 4\pi/\lambda \sin(\theta)$, where $\lambda$ is the X-ray wavelength, and $2\theta$ is the scattering angle) of 0.08–6.1 $nm^{-1}$ at a beam size of $120 \times 370$ µm. The samples were loaded into borosilicate glass capillaries at 25 °C and 2D scattering patterns were collected with an exposure time of 5 s per frame with 2 s delay between three frames on a Pilatus3 2M detector with an active area of $254 \times 289$ $mm^2$ and a pixel size of $172 \times 172$ $\mu m^2$ (Dectris, Baden, Switzerland). The 2D scattering frames were radially integrated into 1D scattering curves, plotted as a function of relative intensity, $I$ versus $q$ using Dawn version 2.7. The triplicates were then inspected to confirm that no beam damage occurred, and averaged. Scattering from water or buffer was subtracted from all samples as background.

*Analysis of SAXS Data*: The cubic space groups were determined by the relative positions of the Bragg peaks displayed in the scattering curves, which correspond to the reflections on planes defined by their (*hkl*) Miller indices. For particles of arbitrary shape with an electron density or scattering length density difference of $\Delta\rho(r)$ relative to the mean value, the pair-distance distribution function $p(r)$ is given by $p(r) = r^2\Delta\tilde{\rho}^2(r)$ where $\Delta\tilde{\rho}^2(r)$ is the convolution square of $\Delta\tilde{\rho}(r)$ averaged for all directions in space. This averaging causes no loss of information in the case of particles with special symmetry. The $p(r)$ is calculated from the scattered intensity $I(q)$ using Equation (2). It can be calculated from experimental data by the indirect Fourier transformation (IFT) method and enables the determination of the overall shape and size of the scattering objects[31]

$$I(q) = 4\pi \int_0^\infty p(r) \frac{\sin qr}{qr} dr \quad (2)$$

The $p(r)$ was characteristic for flat, inhomogeneous structures, e.g., bilayers with a thickness of the bilayer being very small compared to the vesicle diameter. This was further supported by the $q^{-2}$ upturn at low $q$ values.

*Antimicrobial Assays*: The antibacterial activity of the GMO/LL-37 nano-objects at 50/50 w/w ratio were assessed against five different bacteria strains: Gram-negative (*E. coli DSMZ 30083, P. aeruginosa CIP A22 DSMZ 25123*) and Gram-positive (*S. aureus DSMZ 20231, S. epidermis ATCC 4961, B. Subtilis ATCC 6633 OD0.108*). For each strain, the minimum inhibition concentration (MIC) was evaluated before the time-killing assays were performed. Concentration series of GMO/LL-37, GMO/LL-37/F127 and LL-37 between 2 and 250 µg $mL^{-1}$ were prepared. The bacterial strains were grown in brain-heart-infusion (BHI) medium (Sigma-Aldrich, Buchs, Switzerland) overnight. The overnight cultures were adjusted to contain $5.5 \times 10^5$ (CFU $mL^{-1}$), from which 900 µL were added to the test tubes and each test tube treated with the 100 µL of the different formulations varying in concentration. The tubes were kept at 30 °C under shaking at 500 rpm (Eppendorf Mixmate Microplate Shaker). Cell viability was assessed by taking out 50 µL of the bacterial suspensions after 175 min of treatment, serially diluting them with 0.01 M PBS at pH 7.4 and plating 5 µL of the resulting dilutions in triplicates on Tryptic Soy Agar (TSA) plates. After overnight incubation at 37 °C, the CFU were quantified with a Scan 300 automatic colony counter (Interscience, Saint Nom, France). All experiments were conducted in triplets, and the results were averaged.

*Time-killing assays* of the GMO/LL-37 self-assemblies in presence and absence of the hydrophilic stabilizer F127 were performed against the five bacterial strains reported above. For each strain, the bacteria were grown overnight on TSA plates, a few of the single emerging colonies were transferred to 25% BHI medium at pH 7.4 for another overnight incubation. The overnight cultures were then used to inoculate fresh 1% BHI medium (1 mL of overnight culture in 8 mL of 1% BHI) and were incubated for additional 2–3 h until they reached their mid-exponential growth phase. All incubations took place at 37 °C on an orbital shaker

at 160 rpm. The bacterial cultures were then centrifuged at 13 000 × *g* for 3 min and washed with 1% BHI. The bacteria concentration in 1% BHI media was adjusted to $5.5 \times 10^5$ CFU $mL^{-1}$ according to turbidity measurements at OD595, using a BioPhotometer plus (Eppendorf AG, Hamburg, Germany). 900 µL of the resulting cultures were transferred into Protein LoBind Tubes (Eppendorf, Hamburg, Germany) and treated with different final concentrations of LL-37 between 16 and 64 µg $mL^{-1}$. Solutions of PBS, GMO (64 µg $mL^{-1}$) and free LL-37 were used as controls. The tubes were kept at 37 °C under shaking at 500 rpm on a microplate shaker. Cell viability was assessed by taking out 50 µL of the bacterial suspensions after 10, 30, 60, 120, 180, 1200 min of treatment, serially diluting them with 0.01 M PBS at pH 7.4 and plating 5 µL of the resulting dilutions in triplicates on TSA plates. After overnight incubation at 37 °C, the CFU were quantified with a Scan 300 automatic colony counter (Interscience, Saint Nom, France). All experiments were conducted in triplets, and the results were averaged.

*Cell Viability and Proliferation Assays*: Cellular viability was analyzed by Live/Dead (ThermoFisher Scientific, L3224, USA) and Alamar Blue assay (Invitrogen, ThermoFisher scientific, DAL1025, USA). HDF cells (CELLnTEC Advanced Cell Systems AG, Switzerland) were seeded at a concentration of $5 \times 10^3$ per well in 100 µL Dulbecco's Modified Eagle Medium (DMEM) supplemented with 10% fetal bovine serum (FBS) and 1% penicillin/streptomycin in 96-well plates. THP-1 (EACC, England) cells were cultured in RPMI medium containing 10% FBS and 1% penicillin/streptomycin. THP-1 cells were differentiated into macrophages with $100 \times 10^{-9}$ M of phorbol 12-myristate 13-acetate (PMA, Sigma) for 72 h. Differentiated THP-1 cells were kept for 24 h in culture media without PMA to enhance cell viability. Both cell types were cultured for 24 h before stimulation. Cell viability assay was performed for GMO cubosomes (64 µg $mL^{-1}$), LL-37 (64 µg $mL^{-1}$), F127 (0.64 µg $mL^{-1}$), and their combinations prepared in cell culture medium just before the viability assay. Cells in PBS were used as control.

For the Alamar Blue assay, after 24 h or 72 h of incubation, the cell medium was discarded, and cell culture medium containing Alamar Blue solution was added, and cells were incubated at 37 °C for 4 h. The absorbance was measured with a spectrophotometer (Mithras LB 943 Multimode Reader, Berthold Technologies, Germany) at a wavelength of 570 nm, using 600 nm as a reference wavelength. Statistical analysis was performed using GraphPad Prism (Version 6.02, CA USA).

Cell proliferation was tested with ELISA based BrdU assay (Cell Proliferation ELISA BrdU-colorimetric, Roche, 11647229001) according to the manufacturer's instructions. HDFs were seeded onto a 96-well plate at a density of $5 \times 10^3$ cells per well. The cells were then incubated with the test substances, at 37 °C for 24 h. The BrdU incorporation was measured by absorbance of the samples in an ELISA reader at 370 nm (reference wavelength 492 nm). The assay was repeated three times with eight replicates. Cell proliferation was calculated by taking untreated cells as 100%, and statistical analysis was performed in GraphPad.

Two-way ANOVA was used for comparing viability, and one-way ANOVA was used for proliferation differences between multiple groups. Significant values are indicated as follows; $*p < 0.05$, $**p < 0.01$, $***p < 0.001$, and $****p < 0.0001$. All quantitative data were expressed as mean ± standard deviation. For Live/Dead assay after 72 h of incubation, the cells were stained with Calcein-AM and ethidium homodimer reagents at $2 \times 10^{-6}$ and $4 \times 10^{-6}$ M concentrations in PBS at pH 7.4, respectively. After 30 min of incubation, the cells were visualized using confocal laser scanning microscopy (CLSM, LSM 780, Zeiss, Germany).

*Cell Penetration Assay*: To study the cell penetration of the LL-37 with the nanocarriers, FAM labeled LL-37 (5-(and-6)-Carboxyfluorescein (5,6-FAM), CASLO ApS, Lyngby, Denmark) was incubated with HDF cells for 24 h. Excess LL-37 was removed by extensive washing with PBS. The cells were stained for immunohistochemistry with fluorescent dyes for the nuclei at 1:1000 with 4′,6-diamidino-2-phenylindole (DAPI, Thermo Fisher Scientific) and the actin filaments at 1:40 with phalloidin (Alexa Fluor 647 Phalloidin, Thermo Fisher Scientific). The samples were then visualized by confocal laser scanning microscope (CLSM, LSM 780, Zeiss, Germany).

## Supporting Information

Supporting Information is available

## Acknowledgements

The authors acknowledge the Swiss National Science Foundation (Project 200021_169513) and the Novartis Foundation for Medical-Biological Research, both held by S.S. for funding this study. The authors acknowledge support from the Scientific Center for Optical and Electron Microscopy (ScopeM) for technical assistance and access to cryo-TEM facilities. Authors also thank Luzia Wiesli and Thomas Ramsauer (Empa) for their support during the antimicrobial studies.

## Conflict of Interest

The authors declare no conflict of interest.

## Keywords

antibacterial nanocarriers, antimicrobial peptides, cell proliferation, SAXS, stabilizer-free cubosomes

[1] a) A. Giuliani, G. Pirri, S. Nicoletto, *Open Life Sci.* **2007**, *2*, 1; b) M. Mahlapuu, J. Håkansson, L. Ringstad, C. Björn, *Front. Cell. Infect. Microbiol.* **2016**, *6*, 194.

[2] a) A. Peschel, H.-G. Sahl, *Nat. Rev. Microbiol.* **2006**, *4*, 529; b) J. L. Fox, *Nat. Biotechnol.* **2013**, *31*, 379; c) Y. Lai, R. L. Gallo, *Trends Immunol.* **2009**, *30*, 131.

[3] a) R. E. W. Hancock, G. Diamond, *Trends Microbiol.* **2000**, *8*, 402; b) R. Ramos, J. P. Silva, A. C. Rodrigues, R. Costa, L. Guardão, F. Schmitt, R. Soares, M. Vilanova, L. Domingues, M. Gama, *Peptides* **2011**, *32*, 1469.

[4] U. H. N. Dürr, U. S. Sudheendra, A. Ramamoorthy, *Biochim. Biophys. Acta, Biomembr.* **2006**, *1758*, 1408.

[5] a) A. Kasus-Jacobi, S. Noor-Mohammadi, G. L. Griffith, H. Hinsley, L. Mathias, H. A. Pereira, *J. Leukocyte Biol.* **2015**, *97*, 341; b) M. L. Mangoni, A. M. McDermott, M. Zasloff, *Exp. Dermatol.* **2016**, *25*, 167; c) W.-Y. Chen, H.-Y. Chang, J.-K. Lu, Y.-C. Huang, S. G. Harroun, Y.-T. Tseng, Y.-J. Li, C.-C. Huang, H.-T. Chang, *Adv. Funct. Mater.* **2015**, *25*, 7189.

[6] M. D. Seo, H. S. Won, J. H. Kim, T. Mishig-Ochir, B. J. Lee, *Molecules* **2012**, *17*, 12276.

[7] a) B. S. Pattni, V. V. Chupin, V. P. Torchilin, *Chem. Rev.* **2015**, *115*, 10938; b) S. Salentinig, M. Zabara, P. Parisse, H. Amenitsch, *Phys. Chem. Chem. Phys.* **2018**, *20*, 21903.

[8] a) A. Yaghmur, O. Glatter, *Adv. Colloid Interface Sci.* **2009**, *147–148*, 333; b) I. D. Azmi, S. M. Moghimi, A. Yaghmur, *Ther. Delivery* **2015**, *6*, 1347; c) A. Zabara, R. Mezzenga, *J. Controlled Release* **2014**, *188*, 31; d) M. B. Gontsarik, M. T., A. Yaghmur, Q. Ren, K. Maniura-Weber, S. Salentinig, *J. Phys. Chem. Lett.* **2016**, *7*, 3482; e) M. Gontsarik, M. Mohammadtaheri, A. Yaghmur, S. Salentinig, *Biomater. Sci.* **2018**, *6*, 803; f) L. Boge, H. Bysell, L. Ringstad, D. Wennman, A. Umerska, V. Cassisa, J. Eriksson, M.-L. Joly-Guillou, K. Edwards, M. Andersson, *Langmuir* **2016**, *32*, 4217;

g) L. Boge, A. Umerska, N. Matougui, H. Bysell, L. Ringstad, M. Davoudi, J. Eriksson, K. Edwards, M. Andersson, *Int. J. Pharm.* **2017**, *526*, 400; h) T. G. Meikle, A. Zabara, L. J. Waddington, F. Separovic, C. J. Drummond, C. E. Conn, *Colloids Surf., B* **2017**, *152*, 143.

[9] a) G. Popescu, J. Barauskas, T. Nylander, F. Tiberg, *Langmuir* **2007**, *23*, 496; b) A. J. Tilley, C. J. Drummond, B. J. Boyd, *J. Colloid Interface Sci.* **2013**, *392*, 288; c) J. Y. T. Chong, X. Mulet, L. J. Waddington, B. J. Boyd, C. J. Drummond, *Soft Matter* **2011**, *7*, 4768; d) C. J. F. Drummond, *Curr. Opin. Colloid Interface Sci.* **1999**, *4*, 449; e) J. Zhai, T. M. Hinton, L. J. Waddington, C. Fong, N. Tran, X. Mulet, C. J. Drummond, B. W. Muir, *Langmuir* **2015**, *31*, 10871.

[10] a) I. D. M. Azmi, P. P. Wibroe, L.-P. Wu, A. I. Kazem, H. Amenitsch, S. M. Moghimi, A. Yaghmur, *J. Controlled Release* **2016**, *239*, 1; b) P. P. Wibroe, I. D. Mat Azmi, C. Nilsson, A. Yaghmur, S. M. Moghimi, *Nanomedicine* **2015**, *11*, 1909; c) Y. C. Cho, P. J. Pak, Y. H. Joo, H.-S. Lee, N. Chung, *Sci. Rep.* **2016**, *6*, 38884; d) T. M. Hinton, F. Grusche, D. Acharya, R. Shukla, V. Bansal, L. J. Waddington, P. Monaghan, B. W. Muir, *Toxicol. Res.* **2014**, *3*, 11; e) N. Tran, X. Mulet, A. M. Hawley, T. M. Hinton, S. T. Mudie, B. W. Muir, E. C. Giakoumatos, L. J. Waddington, N. M. Kirby, C. J. Drummond, *RSC Adv.* **2015**, *5*, 26785.

[11] I. Hamad, A. C. Hunter, S. M. Moghimi, *J. Controlled Release* **2013**, *170*, 167.

[12] U. Bazylińska, J. Kulbacka, J. Schmidt, Y. Talmon, S. Murgia, *J. Colloid Interface Sci.* **2018**, *522*, 163.

[13] C. V. Kulkarni, W. Wachter, G. Iglesias-Salto, S. Engelskirchen, S. Ahualli, *Phys. Chem. Chem. Phys.* **2011**, *13*, 3004.

[14] a) S. Salentinig, *Curr. Opin. Colloid Interface Sci.* **2019**, *39*, 190; b) S. Salentinig, L. Sagalowicz, O. Glatter, *Langmuir.* **2010**, *26*, 11670.

[15] O. Glatter, *Acta Phys. Austriaca.* **1980**, *52*, 243.

[16] a) A. Yaghmur, P. Laggner, M. Almgren, M. Rappolt, *PLoS One.* **2008**, *3*, e3747; b) A. Yaghmur, L. de Campo, L. Sagalowicz, M. E. Leser, O. Glatter, *Langmuir* **2006**, *22*, 9919.

[17] T. J. Silhavy, D. Kahne, S. Walker, *Cold Spring Harbor Perspect. Biol.* **2010**, *2*, a000414.

[18] K. A. Sochacki, K. J. Barns, R. Bucki, J. C. Weisshaar, *Proc. Natl. Acad. Sci. USA* **2011**, *108*, E77.

[19] H. Thadepalli, S. M. A. Lou, V. T. Bach, T. K. Matsui, A. K. Mandal, *Am. J. Surg.* **1979**, *138*, 845.

[20] M. Claire, L. Wan Li, G. Abhishek, A. Mohd Cairul Iqbal Mohd, R. Iza, T. B. Stephen, R. Prem, K. Ken, *Curr. Opin. Pharmacol.* **2015**, *21*, 43.

[21] a) M. R. Nejadnik, H. C. van der Mei, W. Norde, H. J. Busscher, *Biomaterials* **2008**, *29*, 4117; b) I. Cringus-Fundeanu, J. Luijten, H. C. van der Mei, H. J. Busscher, A. J. Schouten, *Langmuir* **2007**, *23*, 5120; c) A. Roosjen, H. J. Kaper, H. C. van der Mei, W. Norde, H. J. Busscher, *Microbiology* **2003**, *149*, 3239; d) L. H. Marsh, M. Coke, P. W. Dettmar, R. J. Ewen, M. Havler, T. G. Nevell, J. D. Smart, J. R. Smith, B. Timmins, J. Tsibouklis, C. Alexander, *J. Biomed. Mater. Res.* **2002**, *61*, 641; e) C. G. P. H. Schroen, M. A. C. Stuart, K. van der Voort Maarschalk, A. van der Padt, K. van't Riet, *Langmuir* **1995**, *11*, 3068.

[22] a) A. Banerjee, J. Qi, R. Gogoi, J. Wong, S. Mitragotri, *J. Controlled Release* **2016**, *238*, 176; b) Y. Li, M. Kroger, W. K. Liu, *Nanoscale* **2015**, *7*, 16631; c) W. H. De Jong, W. I. Hagens, P. Krystek, M. C. Burger, A. J. A. M. Sips, R. E. Geertsma, *Biomaterials* **2008**, *29*, 1912.

[23] K. Yang, Y.-Q. Ma, *Nat. Nanotechnol.* **2010**, *5*, 579.

[24] Z. Zhu, J. Ding, Z. Ma, T. Iwashina, E. E. Tredget, *Wound Repair Regener.* **2017**, *25*, 377.

[25] E. Dohle, I. Bischoff, T. Bose, A. Marsano, A. Banfi, R. E. Unger, C. J. Kirkpatrick, *Eur. Cells Mater.* **2014**, *27*, 149.

[26] a) Q. Gao, Q. Liang, F. Yu, J. Xu, Q. Zhao, B. Sun, *Colloids Surf., B* **2011**, *88*, 741; b) R. Basak, R. Bandyopadhyay, *Langmuir* **2013**, *29*, 4350.

[27] a) W. Wang, J. Jia, C. Li, Q. Duan, J. Yang, X. Wang, R. Li, C. Chen, H. Yan, Y. Zheng, *Oncol. Lett.* **2016**, *12*, 1745; b) J. M. Kahlenberg, M. J. Kaplan, *J. Immunol.* **2013**, *191*, 4895.

[28] S. Salentinig, S. Phan, T. A. Darwish, N. Kirby, B. J. Boyd, E. P. Gilbert, *Langmuir* **2014**, *30*, 7296.

[29] S. Bolisetty, M. Hoffmann, S. Lekkala, T. Hellweg, M. Ballauff, L. Harnau, *Macromolecules* **2009**, *42*, 1264.

[30] D. Lehner, H. Lindner, O. Glatter, *Langmuir* **2000**, *16*, 1689.

[31] a) O. Glatter, *J. Appl. Crystallogr.* **1980**, *13*, 577; b) J. Brunner-Popela, O. Glatter, *J. Appl. Crystallogr.* **1997**, *30*, 431.